



Buckling Mode Decomposition of Built-up Members by the Modal Finite Strip Method (mFSM)

Mani Khezri¹, Kim J.R. Rasmussen²

Abstract

This paper presents a method to perform the decomposition of the deformed shape of built-up members into the structurally meaningful “pure” modes: local, distortional and global modes. The method is based on the core concept of the authors’ modal finite strip method (mFSM) for single sections, which utilizes normalized strain energies to identify different buckling mode classes. The attention to buckling mode decomposition of built-up sections is motivated by the requirements of the Direct Design Method (DSM) to identify and calculate the buckling loads of the pure local and distortional modes. The presence of discrete fasteners in built-up sections influences the overall buckling behavior and changes the buckling modes. In this study, the mFSM is further developed to achieve a complete decomposition technique that accounts for discrete fasteners. The proposed method is verified against finite element and finite strip solutions through numerical examples and shown to be accurate. The obtained results show that the proposed method can be a valuable tool for the assessment of the behavior of built-up members and their design.

1. Introduction

Cold-formed steel (CFS) sections possess high strength-to-weight ratios and can be easily integrated with other construction materials, making them a versatile choice in the building industry. They can be utilized in a variety of applications, ranging from basic roof-sheeting to low-rise building frames. By connecting multiple component sections to form a built-up cross-section, CFS sections can potentially be extended to mid-rise construction, opening up new opportunities for their use. CFS members are prone to the local and distortional buckling of the cross-section and the interaction of these modes with global buckling modes such as flexural and flexural-torsional modes. As a result, accurately assessing the structural capacity of such members requires evaluating their linear buckling behavior, including identifying the relevant buckling modes and corresponding loads. However, analyzing the buckling behavior becomes increasingly challenging as the cross-section shape becomes more intricate, and it may not always be possible to determine the minimum buckling loads of critical modes, as typically obtained from signature curves generated by standard finite strip analyses. For built-up members, the problem is even more complex as discrete fasteners can significantly alter the local, distortional and global buckling

¹ Lecturer, The University of Sydney, <mani.khezri@sydney.edu.au>

² Professor, The University of Sydney, <kim.rasmussen@sydney.edu.au>

behavior of the member. To efficiently analyze and interpret the complex nature of instabilities encountered in thin-walled structures, decomposition and superposition techniques are required. They involve decomposing the deformed buckled shape of a thin-walled member into a number of "basic" modes that govern the failure load. The development and extension of numerical methods such as generalised beam theory (GBT) (Dinis, Camotim, and Silvestre 2006; Gonçalves, Ritto-Corrêa, and Camotim 2010), constrained finite strip method (cFSM) (Ádány and Schafer 2008; Rendall, Hancock, and Rasmussen 2017), constrained finite element method (Ádány 2018; Ádány, Visy, and Nagy 2018) and modal finite strip method (mFSM) (Khezri and Rasmussen 2019b, 2019a) have been important steps in achieving this objective. To the best of the authors' knowledge, these methods are only applicable to single section members and hence, the problem of modal decomposition of the buckling modes of built-up members has not been yet addressed. In this study, the mFSM is extended to procure a complete decomposition technique that accounts for discrete fasteners and can be employed to built-up sections. This study is founded on the authors' previous work on the compound strip method (Abbasi et al. 2018), which was proposed for the finite strip analysis of built-up sections, and the mFSM (Khezri and Rasmussen 2019b, 2019a). A brief review of these methods is presented in Sections 3 and 4 to provide an insight into their underpinning numerical framework.

Various methods have been developed to analyze the behavior of thin-walled structures, including the compound strip method (CSM) introduced by (Puckett and Gutkowski 1986). The CSM incorporates the stiffness of elastic supporting elements such as columns, and longitudinal and transverse beams in a direct formulation to enhance the versatility and capability of the finite strip method (FSM). The CSM has been employed in linear flexural (Puckett 1986) and buckling (Puckett, Wiseman, and Chong 1987) analyses of straight continuous flat plates over flexible supports. (Borković, Mrđa, and Kovačević 2013) used the CSM to study the linear transient vibration of stiffened plates, where the strain and kinetic energies of stiffeners were added to those of finite strips. (Maleki 1991) extended the application of the CSM to the analysis of folded plates and box girders with intermediate non-rigid supports, while (Borković et al. 2017) utilized the CSM for the geometric nonlinear static analysis of prismatic shells with internal supports and stiffeners.

Puckett and Wiseman (1991) developed a technique for the inclusion of bracing elements in the analysis of folded plates using the CSM. Moreover, the spline compound strip method (SCSM) (Chen, Gutkowski, and Puckett 1991), which is a more versatile extension of the conventional CSM, has been employed in the analysis of stiffened plates and braced thin-walled structures. In this study, the compound strip method, as developed by the authors (Abbasi et al. 2018), is employed for the buckling analysis of built-up cold-formed steel (CFS) members, where the discrete fasteners are modeled as connecting elements with adjustable stiffness properties.

Modal decomposition numerical methods (e.g. cFSM, and cFEM) impose specific kinematic constraints formulated to suit the method being used (e.g. FSM, and FEM). However, this approach requires significant modification of the constraint matrices for different methods, even though they share the same underlying kinematic assumptions based on GBT mechanics. Recently, the authors proposed a novel decomposition method (mFSM) in which the pure modes are categorized based on the participation of specific components of the bending and membrane strain energies. The distinct feature of the mFSM is that because it operates on strain energy, it can be readily extended

to the buckling mode decomposition of members with complex cross-sections. In this study, the CSM and mFSM are combined and accordingly modified to derive a novel method for the modal decomposition of the buckling modes of built-up members.

The outline of this paper is as follows. In Section 2, the semi-analytical finite strip method (FSM) and its application to the buckling analysis of thin-walled prismatic members is briefly reviewed. In Section 3, the compound strip method and its application to model discrete fasteners in built-up sections are explained. In Section 4, the core concept of the proposed modal decomposition method mFSM is clarified and the required modification in the formulation for built-up sections is set out. A series of numerical examples are included in Section 5 to demonstrate the accuracy and versatility of the mFSM in capturing the modal behavior of built-up thin-walled members.

2. Finite strip buckling analysis

2.1 The semi-analytical finite strip method

The FSM divides a thin-walled member transversely into (ns) strips using (n) nodal lines, as seen in Fig. 1, and uses analytical functions such as beam eigenfunctions (Cheung and Cheung 1971) or trigonometric functions (Bradford and Azhari 1995) to describe the displacements of the strips in the longitudinal direction, while polynomial shape functions are used in the transverse direction.

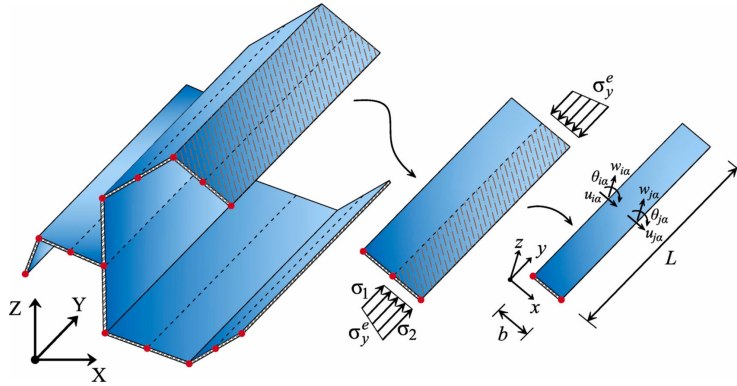


Figure 1: Strip discretization and DOFs, local and global coordinates systems, and nomenclature.

The general displacement functions for an arbitrary point (x,y) on the mid-surface of the strip depicted in Fig. 1 can be expressed as follows:

$$\begin{aligned} u_s(x, y) &= \sum_{\alpha=1}^P (\psi_{mu}(x) \mathbf{d}_{m\alpha}^s) S_{\alpha}(y), \\ v_s(x, y) &= \sum_{\alpha=1}^P (\psi_{mv}(x) \mathbf{d}_{m\alpha}^s) \frac{1}{\mu_{\alpha}} S_{\alpha,y}(y), \\ w_s(x, y) &= \sum_{\alpha=1}^P (\psi_b(x) \mathbf{d}_{b\alpha}^s) S_{\alpha}(y), \end{aligned} \quad (1)$$

in which P is the number of terms utilized in the longitudinal direction, S_{α} is the α th term of the harmonic function series, μ_{α} is the coefficient for the argument of α th term, and $\mathbf{d}_{m\alpha}^s$ and $\mathbf{d}_{b\alpha}^s$ are vectors of degrees of freedom (DOFs) for membrane and bending displacements, respectively.

2.2 Internal elastic strain energy and strip stiffness matrices

The flat strip shown in Fig. 1 is assumed to maintain its flatness in the presence of applied stresses until it reaches the point of buckling. The strip total strain energy is defined as follows:

$$U^s = \frac{1}{2} \int_V (\boldsymbol{\sigma}^s)^T \boldsymbol{\varepsilon}^s dV, \quad (2)$$

and can be expressed as the sum of the strain energies associated with membrane and bending deformations:

$$U^s = \underbrace{\sum_{\alpha=1}^P \sum_{\beta=1}^P \frac{1}{2} (\mathbf{d}_{m\alpha}^s)^T \mathbf{k}_{m\alpha\beta}^s \mathbf{d}_{m\beta}^s}_{U_m^s} + \underbrace{\sum_{\alpha=1}^P \sum_{\beta=1}^P \frac{1}{2} (\mathbf{d}_{b\alpha}^s)^T \mathbf{k}_{b\alpha\beta}^s \mathbf{d}_{b\beta}^s}_{U_b^s}, \quad (3)$$

in which $\mathbf{k}_{m\alpha\beta}^s$ and $\mathbf{k}_{b\alpha\beta}^s$ are the strip membrane and flexural stiffness matrices, obtained as:

$$\mathbf{k}_{m\alpha\beta}^s = \iint_{L \ b} (\mathbf{B}_{m\alpha}^s)^T \mathbf{D}_m \mathbf{B}_{m\alpha}^s t \, dx \, dy, \quad \mathbf{k}_{b\alpha\beta}^s = \iint_{L \ b} (\mathbf{B}_{b\alpha}^s)^T \mathbf{D}_b \mathbf{B}_{b\alpha}^s \, dx \, dy. \quad (4)$$

In Eq. (4), \mathbf{D}_m and \mathbf{D}_b are membrane and bending property matrices, respectively, and $\mathbf{B}_{m\alpha}^s$ and $\mathbf{B}_{b\alpha}^s$ are membrane and bending strain compliance matrices, respectively, (Cheung and Cheung 1971). Using Eq. (4), the strip stiffness matrix corresponding to the half-waves α and β is obtained by assembling the membrane and bending components:

$$\mathbf{k}_{\alpha\beta}^s = \begin{bmatrix} \mathbf{k}_{m\alpha\beta}^s & 0 \\ 0 & \mathbf{k}_{b\alpha\beta}^s \end{bmatrix}. \quad (5)$$

Thus, the total strain energy of the strip can be expressed as

$$U^s = \sum_{\alpha=1}^P \sum_{\beta=1}^P \frac{1}{2} (\mathbf{d}_{\alpha}^s)^T \mathbf{k}_{\alpha\beta}^s \mathbf{d}_{\beta}^s = \frac{1}{2} (\mathbf{d}^s)^T \mathbf{k}^s \mathbf{d}^s, \quad \text{where } \mathbf{k}^s = \begin{bmatrix} \mathbf{k}_{11}^s & \cdots & \mathbf{k}_{1P}^s \\ \vdots & \ddots & \vdots \\ \mathbf{k}_{P1}^s & \cdots & \mathbf{k}_{PP}^s \end{bmatrix}, \quad \text{and } \mathbf{d}^s = \begin{Bmatrix} \mathbf{d}_1^s \\ \vdots \\ \mathbf{d}_P^s \end{Bmatrix}. \quad (6)$$

2.3 Potential energy of external loads and strip stability matrices

The reduction in potential energy of in-plane stresses $\boldsymbol{\sigma}_m^e$ caused by the buckling deformation of a flat strip can be expressed as:

$$V^s = \int_V \boldsymbol{\varepsilon}_{NL}^T \boldsymbol{\sigma}_m^e dV, \quad (7)$$

in which $\boldsymbol{\varepsilon}_{NL}$ is the nonlinear component of the membrane strain vector, defined as (Plank and Wittrick 1974):

$$\boldsymbol{\varepsilon}_{NL} = \left\{ \frac{1}{2} \left(\frac{\partial w}{\partial x} \right)^2, \frac{1}{2} \left(\frac{\partial u}{\partial y} \right)^2 + \frac{1}{2} \left(\frac{\partial v}{\partial y} \right)^2 + \frac{1}{2} \left(\frac{\partial w}{\partial y} \right)^2, \left(\frac{\partial w}{\partial x} \right) \left(\frac{\partial w}{\partial y} \right) \right\}^T. \quad (8)$$

Considering only strips subjected to longitudinal in-plane stresses, one can rewrite the Eq. (7) as follows,

$$V^s = \int_V \frac{1}{2} \left[\left(\frac{\partial u}{\partial y} \right)^2 + \left(\frac{\partial v}{\partial y} \right)^2 \right] \sigma_y^e dV + \int_V \frac{1}{2} \left(\frac{\partial w}{\partial y} \right)^2 \sigma_y^e dV. \quad (9)$$

Utilizing the general displacement functions given in Eq. (1), and by appropriate differentiation, one obtains,

$$V^s = \sum_{\alpha=1}^P \sum_{\beta=1}^P \frac{1}{2} (\mathbf{d}_{m\alpha}^s)^\top \overbrace{\left(\int_L \int_b \sigma_y^e (\mathbf{G}_{m\alpha}^s)^\top \mathbf{G}_{m\beta}^s t dx dy \right)}^{\mathbf{g}_{m\alpha\beta}^s} \mathbf{d}_{m\beta}^s + \frac{1}{2} (\mathbf{d}_{b\alpha}^s)^\top \overbrace{\left(\int_L \int_b \sigma_y^e (\mathbf{G}_{b\alpha}^s)^\top \mathbf{G}_{b\beta}^s t dx dy \right)}^{\mathbf{g}_{b\alpha\beta}^s} \mathbf{d}_{b\beta}^s, \quad (10)$$

in which $\mathbf{g}_{m\alpha\beta}^s$ and $\mathbf{g}_{b\alpha\beta}^s$ are the strip membrane and bending stability matrices, respectively, corresponding to α th and β th terms. Similar to the stiffness matrix, the strip stability matrix for the α th and β th terms is defined as,

$$\mathbf{g}_{\alpha\beta}^s = \begin{bmatrix} \mathbf{g}_{m\alpha\beta}^s & 0 \\ 0 & \mathbf{g}_{b\alpha\beta}^s \end{bmatrix}. \quad (11)$$

The strip stability matrix allows the potential energy of the externally applied loads to be written as,

$$V^s = \sum_{\alpha=1}^P \sum_{\beta=1}^P \frac{1}{2} (\mathbf{d}_\alpha^s)^\top \mathbf{g}_{\alpha\beta}^s \mathbf{d}_\beta^s = \frac{1}{2} (\mathbf{d}^s)^\top \mathbf{g}^s \mathbf{d}^s, \text{ where } \mathbf{g}^s = \begin{bmatrix} \mathbf{g}_{11}^s & \cdots & \mathbf{g}_{1P}^s \\ \vdots & \ddots & \vdots \\ \mathbf{g}_{P1}^s & \cdots & \mathbf{g}_{PP}^s \end{bmatrix}. \quad (12)$$

2.4 Global stiffness and stability matrices

The strip stability and stiffness matrices described in Eqs. (6) and (12) were derived in the local coordinate system assigned to the strip. To construct the global stiffness (\mathbf{K}) and stability (\mathbf{G}) matrices for a member containing multiple strips (Fig. 1), the matrices based on local coordinates need to be transformed to global coordinates and subsequently assembled according to the connectivity of the strips. Likewise, the local strip displacement vectors \mathbf{d}_s (Eq. (6)) need to be transformed to global coordinates and assembled into the global displacement vector \mathbf{d} .

2.5 Buckling equation

The total potential energy (Π) is the sum of the internal elastic energy (U) and the reduction in potential energy resulting from the work of external actions (V):

$$\Pi = U - V. \quad (13)$$

Expressed in terms of the assembled global stiffness and stability matrices, the internal strain energy and potential energy due to the work of external loads can be written as follows:

$$U = \frac{1}{2} \mathbf{d}^\top \mathbf{K} \mathbf{d}, \quad (14)$$

$$V = \frac{1}{2} \mathbf{d}^\top \mathbf{G} \mathbf{d}. \quad (15)$$

Substituting Eqs. (14) and (15) into Eq. (13), the relation for the total potential energy of the thin-walled member is derived as,

$$\Pi = \frac{1}{2} \mathbf{d}^T \mathbf{K} \mathbf{d} - \frac{1}{2} \mathbf{d}^T \mathbf{G} \mathbf{d} = \frac{1}{2} \mathbf{d}^T (\mathbf{K} - \lambda \mathbf{G}_u) \mathbf{d}, \quad (16)$$

where λ is a load factor that scale the stability matrix obtained for reference external loads (\mathbf{G}_u) to the stability matrix of the member (\mathbf{G}) under actual external loads. Minimizing the total potential energy of Eq. (16) with respect to \mathbf{d} results in the well-known buckling eigenvalue equation:

$$(\mathbf{K} - \Lambda \mathbf{G}_u) \Phi = \mathbf{0}, \quad (17)$$

where Λ represents the diagonal matrix containing the eigenvalues of the problem and Φ is the eigenmode matrix.

3. Compound strip method for the analysis of built-up sections

The authors (Abbasi et al. 2018; Khezri, Abbasi, and Rasmussen 2017) proposed a framework for analyzing built-up sections with discrete fasteners (Fig. 2(a)), in which the fasteners are modelled as connecting elements with adjustable stiffness properties. The approach provides a simple yet accurate numerical tool that can accommodate any desired cross-sectional composition and fastener configuration, thereby facilitating extensive parametric studies and providing a useful tool for structural design. The fasteners are modelled as three-dimensional beam elements with three translational and three rotational DOFs at each end (Fig. 2(b)).

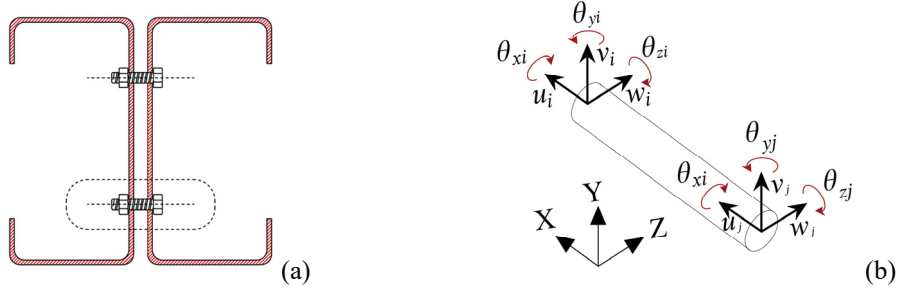


Figure 2. (a) Schematic view of a built-up section with discrete fasteners, (b) local coordinates and degrees of freedom of an arbitrarily oriented connection element.

The relationship between the nodal force and nodal displacement vectors for a fastener is expressed in the local coordinate system of the element as follows:

$$\begin{Bmatrix} \mathbf{F}_i \\ \mathbf{F}_j \end{Bmatrix} = \begin{bmatrix} \mathbf{K}_{ii} & \mathbf{K}_{ij} \\ \mathbf{K}_{ji} & \mathbf{K}_{jj} \end{bmatrix} \begin{Bmatrix} \delta_i \\ \delta_j \end{Bmatrix} = \mathbf{K}_c \delta_c, \quad (18)$$

where,

$$\delta_\mu = \{u_\mu \quad v_\mu \quad w_\mu \quad \theta_{x\mu} \quad \theta_{y\mu} \quad \theta_{z\mu}\}^T, \quad \mathbf{F}_\mu = \{F_{x\mu} \quad F_{y\mu} \quad F_{z\mu} \quad M_{x\mu} \quad M_{y\mu} \quad M_{z\mu}\}^T, \quad (\mu = i, j) \quad (19)$$

and \mathbf{K}_c is the stiffness matrix of the connection element. Abbasi et al. (2018) assumed that the flexural behavior of the element is uncoupled in perpendicular planes, and therefore the flexural behavior in each plane can be described by its respective shear and flexural stiffness properties. By utilizing a general set of slope-deflection equations and assuming rigid ends, the sub-matrices of the stiffness matrix in Eq. (18) can be expressed in terms of the in-plane stiffness constants. The

detailed derivation of these matrices for both Euler-Bernoulli and Timoshenko beam elements can be found in (Abbasi et al. 2018).

The connection element is incorporated in the finite strip model by adding its stiffness to the stiffness of the strips, while ensuring compatibility of displacements and rotations between the element and the strips connected by the element. The system being considered comprises two strips with parallel longitudinal axes that are linked by a connection element oriented in an arbitrary manner, as illustrated in Fig. 3.

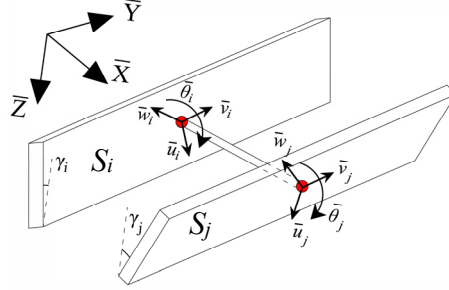


Figure 3. Three-dimensional model for connection element and adjoining constituent strips.

The total strain energy of this system can be calculated as the sum of the strain energies of the flat component strips and the connection element(s), i.e.

$$\Pi = \Pi_{S_i} + \Pi_{S_j} + \sum_{k=1}^{NC} \Pi_{C_k} \quad (20)$$

where Π_{S_i} and Π_{S_j} are the strain energies of the connected strips, NC is the number of connection elements, and Π_{C_k} is the strain energy of the k th element in its local coordinate system, viz.

$$\Pi_{C_k} = \frac{1}{2} \delta_c^T \mathbf{K}_c \delta_c \quad (21)$$

To calculate the strain energy (Π_{C_k}), it is first necessary to express the displacements of the connection elements in terms of the global nodal displacements of the strips. This is achieved by the multiplication of the transformation matrix \mathbf{R} , obtained by superposition of three single-axis rotations of the local coordinate system (Chen, Gutkowski, and Puckett 1991; Wiseman and Puckett 1991). In the next step, the displacements in the global coordinate system $\bar{X}\bar{Y}\bar{Z}$ (Fig. 3) are then transformed to local strip coordinates using the \mathbf{R}_{GL} matrix. As the strips are assumed to be parallel to the \bar{Z} axis, the arrays of the \mathbf{R}_{GL} matrix are functions of the orientation angles (γ_i, γ_j) of the connected strips, (Fig. 3). The last step involves the interpolation of the displacement values of the connection elements based on the displacement field of the strips using interpolation matrices Ψ^{m_μ} and Ψ^{n_μ} ($\mu = i, j$), followed by the conversion of the resulting components into the global coordinate system. The interpolation matrices are formed by using the strip shape functions in the transverse direction and the chosen longitudinal functions for the terms m and n . The above steps can be summarized using matrix notation as follows:

$$\bar{\mathbf{K}}_c^{nm} = \mathbf{R}_{GL} (\Psi^n)^T (\mathbf{R}_{GL})^T \mathbf{R}^T \mathbf{K}_c \mathbf{R} \mathbf{R}_{GL} \Psi^m (\mathbf{R}_{GL})^T \quad (22)$$

The detailed derivation of the aforementioned transformation and interpolation matrices can be found in (Abbasi et al. 2018). The stiffness matrices for the connection elements can be assembled into the stiffness matrix of the system by adding their rows and columns in correspondence with

the global degrees of freedom. As a numerical strategy, which will facilitate the modal decomposition for the built-up sections, we form a separate matrix (\mathbf{K}_{cnts}) with the same size as the stiffness matrix for the whole system, to store the stiffness contributions of the connection elements. Thus, for a built-up member consisting of N single sections, the system stiffness matrix \mathbf{TK} can be obtained as follows:

$$[\mathbf{TK}]_{nt \times nt} = \underbrace{\begin{bmatrix} \mathbf{K}_1 & 0 & \dots & 0 \\ 0 & 0 & \dots & 0 \\ \vdots & \vdots & \ddots & 0 \\ 0 & 0 & 0 & 0 \end{bmatrix}_{nt \times nt}}_{N} + \underbrace{\begin{bmatrix} 0 & 0 & \dots & 0 \\ 0 & \mathbf{K}_2 & \dots & 0 \\ \vdots & \vdots & \ddots & 0 \\ 0 & 0 & 0 & 0 \end{bmatrix}_{nt \times nt}}_{N} + \dots + \underbrace{\begin{bmatrix} 0 & 0 & \dots & 0 \\ 0 & 0 & \dots & 0 \\ \vdots & \vdots & \ddots & 0 \\ 0 & 0 & 0 & \mathbf{K}_N \end{bmatrix}_{nt \times nt}}_{N} + [\mathbf{K}_{cnts}]_{nt \times nt} \quad (23)$$

or,

$$\mathbf{TK} = \mathbf{K} + \mathbf{K}_{cnts} \quad (24)$$

in which, nt is the total number of DOFs.

4. Modal finite strip method (mFSM)

Fundamentally, modal decomposition methods are based on the premise that any arbitrary displacement field can be expressed as a linear combination of modes in pure deformation spaces. These deformation spaces comprise a collection of structurally meaningful "pure" modes that constitute an orthogonal basis, capable of spanning the entire displacement space. Prior research endeavors have utilized the principles and mechanical assumptions of the Generalized Beam Theory (GBT) to formulate these base vectors and to classify them into distinct categories, such as global (G), distortional (D), local (L), shear (S), and transverse extension (TE) spaces (Ádány and Schafer 2014a, 2014b). These spaces can be further divided into subspaces as presented in Table 1.

Table 1: Mechanical criteria for mode classes (Ádány and Schafer 2014a, 2014b)

	G			D	L		S						TE				
	G _A	G _B	G _T		L _P	L _S	S _{Bt}	S _{Tt}	S _{Dt}	S _{Ct}	S _{Bw}	S _{Tw}	S _{Dt}	S _{Cw}	S _{Sw}	TE _P	TE _S
$\varepsilon_x = 0$		Y		Y	Y						Y						N
$\gamma_{xy} = 0$		Y		Y	Y						N						N
Trans. Eq.		Y		Y	N		Y	Y	Y	N	Y	Y	Y	Y	Y		N
$\varepsilon_y = 0$		N		N	Y		Y	Y	Y	N	N	N	N	N	N		Y
$\kappa_x = 0$		Y		N		N	Y	Y	N	N	Y	Y	Y	Y	Y		N Y
$\kappa_y = 0$	Y	Y	N	N	N	N	Y	N	N	N	Y	Y	Y	Y	Y		N Y
$\kappa_{xy} = 0$	Y	N	N	N	N	N	N	N	N	N	Y	Y	Y	Y	Y		N Y

The present study employs the same mechanical criteria for modal identification and classification of deformation modes as those utilized in the generalized constrained Finite Strip Method (cFSM) and in the previously proposed mFSM (Khezri and Rasmussen 2019b, 2019a, 2018). In the generalized cFSM, a set of constraint matrices (\mathbf{R}_M) is defined for each of the deformation subspaces, which facilitate the mapping of the general deformation space (\mathbf{d}) to the constrained space (\mathbf{d}_M), i.e.

$$\mathbf{d} = \mathbf{R}_M \mathbf{d}_M. \quad (25)$$

The columns of the constraint matrix \mathbf{R}_M represent the base vectors of the constrained space and are determined based on the criteria for each mode class. As an eigenmode is a general displacement vector, Eq. (25) can be applied to all eigenvectors in the matrix Φ , as follows:

$$\Phi = \mathbf{R}_M \Phi_M. \quad (26)$$

Thus, using Eq. (26), the constrained eigenvalue problem, for subspace M can be obtained as

$$\left(\mathbf{R}_M^T \mathbf{K} \mathbf{R}_M - \Lambda_M \mathbf{R}_M^T \mathbf{G}_u \mathbf{R}_M \right) \Phi_M = \mathbf{0}, \quad \text{or in short,} \quad \left(\hat{\mathbf{K}}_M - \Lambda_M \hat{\mathbf{G}}_M \right) \Phi_M = \mathbf{0}, \quad (27)$$

in which \mathbf{K} and \mathbf{G}_u are the global stiffness and stability matrices, respectively, and $\hat{\mathbf{K}}_M$ and $\hat{\mathbf{G}}_M$ are the stiffness and stability matrices of the constrained problem, respectively. To enforce the criteria defined in Table 1, which are mainly defined as zero strains (derivatives of displacements), for each space (M), the relations between associated degrees of freedom are established such that the considered strains become zero. It should be noted that following the cFSM approach, the computation of constraint matrices is reliant on the specific choice of general displacement functions and type of element, or more broadly, the numerical method.

In mFSM, an alternative approach is utilized to generate the constraint matrices, or modal base vectors. In this approach, the modal base vectors for each mode class are obtained by solving a generalized eigenvalue problem, which determines the ratio of the elastic strain energy developed under mode M deformations to that of general displacements, i.e.,

$$\Upsilon_M = \frac{\mathbf{H}_M^T \mathbf{K}_M \mathbf{H}_M}{\mathbf{H}_M^T \mathbf{K} \mathbf{H}_M}. \quad (28)$$

In Eq. (28), \mathbf{H}_M represents a matrix of base vectors for the general displacement space, while \mathbf{K}_M represents the stiffness matrix for mode M , constructed based on the kinematic criteria for that mode. It is important to note that additional criteria, such as transverse equilibrium and orthogonality of mode classes, are also satisfied in this method through appropriate adjustments and modifications to the \mathbf{H}_M matrix. To obtain the strain energy ratios required in Eq. (28), the following generalized eigenvalue problem must be solved:

$$\left(\left(\mathbf{H}_M^T \mathbf{K}_M \mathbf{H}_M \right) - \Upsilon_M \left(\mathbf{H}_M^T \mathbf{K} \mathbf{H}_M \right) \right) \Theta_M = \mathbf{0}. \quad (29)$$

The eigenmodes matrix, denoted by Θ_M , is obtained as the solution of the generalized eigenvalue problem described in Eq. (29). The constraint matrix (\mathbf{R}_M) for mode class M is then obtained by extracting the columns of the Θ_M matrix that satisfy the necessary criteria and correspond to zero associated strain energy ratios.

To obtain the modal stiffness matrix (\mathbf{K}_M) that only includes terms associated with specific strains, the internal strain energy is first decomposed into individual terms representing the contributions of each strain component:

$$U = \underbrace{U_{\varepsilon_x} + U_{\varepsilon_y} + U_{\varepsilon_x\varepsilon_y} + U_{\gamma_{xy}}}_{U_m} + \underbrace{U_{\kappa_x} + U_{\kappa_y} + U_{\kappa_x\kappa_y} + U_{\kappa_{xy}}}_{U_b}, \quad (30)$$

in which

$$\begin{aligned} U_{\varepsilon_x} &= \frac{1}{2} \mathbf{d}^T \mathbf{K}_{\varepsilon_x} \mathbf{d}, & U_{\varepsilon_y} &= \frac{1}{2} \mathbf{d}^T \mathbf{K}_{\varepsilon_y} \mathbf{d}, & U_{\varepsilon_x\varepsilon_y} &= \frac{1}{2} \mathbf{d}^T \mathbf{K}_{\varepsilon_x\varepsilon_y} \mathbf{d}, & U_{\gamma_{xy}} &= \frac{1}{2} \mathbf{d}^T \mathbf{K}_{\gamma_{xy}} \mathbf{d}, \\ U_{\kappa_x} &= \frac{1}{2} \mathbf{d}^T \mathbf{K}_{\kappa_x} \mathbf{d}, & U_{\kappa_y} &= \frac{1}{2} \mathbf{d}^T \mathbf{K}_{\kappa_y} \mathbf{d}, & U_{\kappa_x\kappa_y} &= \frac{1}{2} \mathbf{d}^T \mathbf{K}_{\kappa_x\kappa_y} \mathbf{d}, & U_{\kappa_{xy}} &= \frac{1}{2} \mathbf{d}^T \mathbf{K}_{\kappa_{xy}} \mathbf{d}. \end{aligned} \quad (31)$$

The total stiffness matrix of the member can be obtained by adding the stiffness sub-matrices given in Eq. (31), which can be expressed as:

$$\mathbf{K} = \underbrace{\mathbf{K}_{\varepsilon_x} + \mathbf{K}_{\varepsilon_y} + \mathbf{K}_{\varepsilon_x\varepsilon_y} + \mathbf{K}_{\gamma_{xy}}}_{\mathbf{K}_m} + \underbrace{\mathbf{K}_{\kappa_x} + \mathbf{K}_{\kappa_y} + \mathbf{K}_{\kappa_x\kappa_y} + \mathbf{K}_{\kappa_{xy}}}_{\mathbf{K}_b}, \quad (32)$$

The derivation of the member stiffness sub-matrices allows direct enforcement of the criteria in Table 1 that are imposed on strains. The detailed procedure to obtain the required modal base vectors for the defined subspaces, can be found in (Khezri and Rasmussen 2018, 2019b, 2019a).

In this study, the formulation for single section members is extended to built-up members. For a built-up member composed of N single sections, the member stiffness sub-matrices associated with each strain component can be obtained as:

$$\left[\mathbf{K}_{\varepsilon_x} \right] = \begin{bmatrix} \mathbf{K}_{\varepsilon_x}^1 & \cdots & 0 \\ \vdots & \ddots & \vdots \\ 0 & \cdots & \mathbf{K}_{\varepsilon_x}^N \end{bmatrix}, \quad \left[\mathbf{K}_{\varepsilon_y} \right] = \begin{bmatrix} \mathbf{K}_{\varepsilon_y}^1 & \cdots & 0 \\ \vdots & \ddots & \vdots \\ 0 & \cdots & \mathbf{K}_{\varepsilon_y}^N \end{bmatrix}, \quad (33)$$

$$\left[\mathbf{K}_{\varepsilon_x\varepsilon_y} \right] = \begin{bmatrix} \mathbf{K}_{\varepsilon_x\varepsilon_y}^1 & \cdots & 0 \\ \vdots & \ddots & \vdots \\ 0 & \cdots & \mathbf{K}_{\varepsilon_x\varepsilon_y}^N \end{bmatrix}, \quad \left[\mathbf{K}_{\gamma_{xy}} \right] = \begin{bmatrix} \mathbf{K}_{\gamma_{xy}}^1 & \cdots & 0 \\ \vdots & \ddots & \vdots \\ 0 & \cdots & \mathbf{K}_{\gamma_{xy}}^N \end{bmatrix},$$

$$\left[\mathbf{K}_{\kappa_x} \right] = \begin{bmatrix} \mathbf{K}_{\kappa_x}^1 & \cdots & 0 \\ \vdots & \ddots & \vdots \\ 0 & \cdots & \mathbf{K}_{\kappa_x}^N \end{bmatrix}, \quad \left[\mathbf{K}_{\kappa_y} \right] = \begin{bmatrix} \mathbf{K}_{\kappa_y}^1 & \cdots & 0 \\ \vdots & \ddots & \vdots \\ 0 & \cdots & \mathbf{K}_{\kappa_y}^N \end{bmatrix}, \quad (34)$$

$$\left[\mathbf{K}_{\kappa_x\kappa_y} \right] = \begin{bmatrix} \mathbf{K}_{\kappa_x\kappa_y}^1 & \cdots & 0 \\ \vdots & \ddots & \vdots \\ 0 & \cdots & \mathbf{K}_{\kappa_x\kappa_y}^N \end{bmatrix}, \quad \left[\mathbf{K}_{\kappa_{xy}} \right] = \begin{bmatrix} \mathbf{K}_{\kappa_{xy}}^1 & \cdots & 0 \\ \vdots & \ddots & \vdots \\ 0 & \cdots & \mathbf{K}_{\kappa_{xy}}^N \end{bmatrix},$$

In order to obtain the modal base vectors for mode class M for the built-up member, two adjustments need to be made to the generalized eigenvalue problem defined by Eq. (28): (1) In forming the modal stiffness matrix (\mathbf{K}_M), the contributions of all sections of the built-up member are incorporated using Eqs. (33) and (34), but the fasteners stiffness terms are not added to the \mathbf{K}_M

matrix; (2) The system stiffness matrix \mathbf{TK} , which is obtained using Eq. (24) and accounts for the stiffness of fasteners \mathbf{K}_{cnts} , replaces the member stiffness matrix \mathbf{K} in the equation. Thus, the equation that determines the ratio of the elastic strain energy developed under mode M deformations to that of general displacements for a built-up member can be derived as:

$$\Upsilon_M = \frac{\mathbf{H}_M^T \mathbf{K}_M \mathbf{H}_M}{\mathbf{H}_M^T \mathbf{TK} \mathbf{H}_M} = \frac{\mathbf{H}_M^T \mathbf{K}_M \mathbf{H}_M}{\mathbf{H}_M^T (\mathbf{K} + \mathbf{K}_{cnts}) \mathbf{H}_M}. \quad (35)$$

The process of separating pure modes is similar to that explained for single section members analyzed using mFSM (Khezri and Rasmussen 2019b, 2019a). As the global axial space is always the first space to be separated, and no condition of orthogonality with other spaces is required, a suitable choice for the initial \mathbf{H}_M ($M = G_A$) matrix is the range of the eigenmodes matrix $\mathbf{\Phi}$. The eigenmodes matrix is a full rank matrix and thus its range obtained by singular value decomposition (SVD) (Strang 1993) has the same dimensions as $\mathbf{\Phi}$. For the problems considered here, the $\mathbf{\Phi}$ matrix is obtained by solving the buckling problem for the built-up member, i.e. Eq. (17). Selection of this range ensures that the space in which modal decomposition is conducted, is a space compatible with the deformation modes of the built-up member. It is noted that in order to obtain pure modes that satisfy the GBT basic assumptions, the Poisson's effect must be ignored. This can be achieved simply by setting the Poisson's ratio to zero (Ádány et al. 2009). By doing this, the global sub-matrices that account for the interaction of strain components will vanish.

5. Numerical examples

5.1 General

In this section, we investigate the applicability of the proposed modal Finite Strip Method (mFSM) for built-up sections through a series of numerical examples. Initially, the buckling behavior of a single section is evaluated, followed by the utilization of the Compound Strip Method (CSM) to analyze the buckling characteristics of a built-up section composed of multiple single constituent sections. Then, the mFSM is applied for the modal decomposition of the buckling deformations of the single and built-up sections.

5.2 Buckling analysis of a single channel section

This example involves the analysis of a single channel section, denoted as C2.0-90-75 and depicted in Fig.4 (a), under uniform compression. The dimensions of the channel section as well as the relevant elastic material properties are specified in Table 2 and Table 3, respectively.

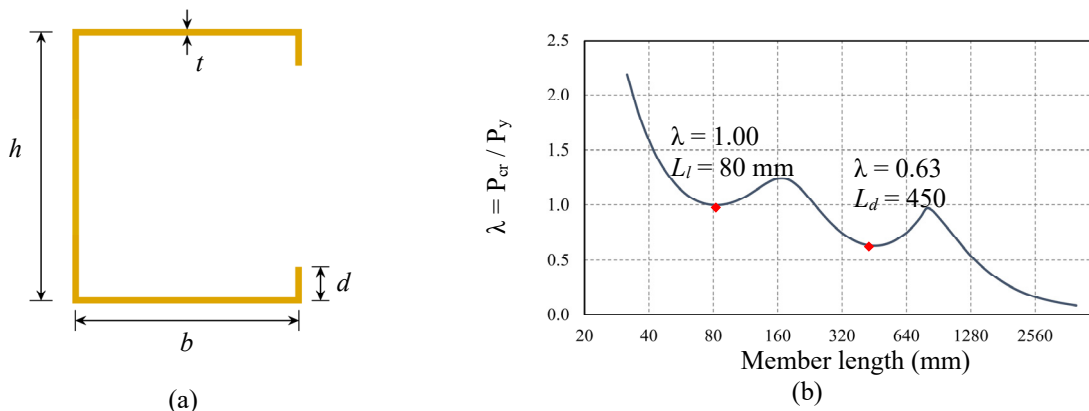


Figure 4: (a) General geometry of a lipped channel section (b) buckling signature curve for the considered section

The investigation considers the end boundary conditions as simply supported. The cross-section is partitioned into strips, with twelve strips employed for the web, eight strips allocated for each flange, and four strips used in each lip. The results obtained for the buckling signature curve ($m = 1$) are shown in Fig. 4(b), where the load factor (λ) is the elastic buckling load P_{cr} normalized with respect to the yield load $P_y = A \cdot f_y$. Fig. 4(b) illustrates that the section signature curve exhibits distinct local and distortional minima at lengths of $L_l = 80$ mm and $L_d = 450$ mm, respectively. The results of the FS analysis using only one term indicate that the section under consideration is susceptible to both local and distortional buckling. This is due to the fact that the elastic local buckling load is greater than the lowest distortional buckling load, which in turn means that the buckling mode transitions from local to distortional as the length of the member increases.

Table 2: Dimensions of channel section.

Section	h (mm)	t (mm)	b (mm)	d (mm)
C2.-90-75	90	2.0	75	12

Table 3: Elastic material properties for cold-formed steel.

Material	E (MPa)	ν (-)	f_y (MPa)
G450	210×10^3	0.3	450

In order to gain a deeper understanding of the buckling behavior of the single section under consideration, the FSM analysis has been repeated with an increased number of longitudinal terms, determined using the feature in CUFSM (Schafer and Adany 2006) that recommends the suitable longitudinal terms for each length. The results obtained are verified against finite element (FE) simulations obtained using ABAQUS software, see Fig. 5. The linear shell element with reduced integration (S4R) was assigned to all plate components. While the enforcement of end boundary conditions in the FSM is achieved by using analytical functions that satisfy the support conditions a priori, in FE models, the boundary conditions must be prescribed explicitly. In this study, the modelling procedure described in (Abbasi et al. 2018) was used to specify simply supported boundary conditions in the FE model. It allows free in-plane expansion of each plate component at the supports and enables direct comparison with buckling loads obtained from a FS analysis.

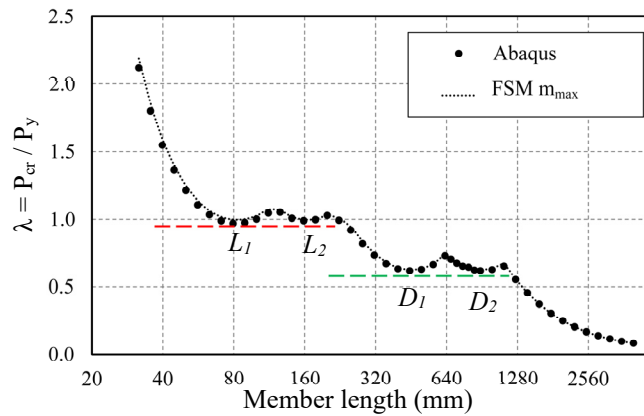


Figure 5: Buckling load curves of the channel section obtained using FSM and FE analyses.

As can be seen in Fig. 5, the inclusion of a larger number of longitudinal terms captures another two local and distortional minima (L_2 , and D_2) in addition to those depicted in the signature curve.

The FSM analysis reveals that the buckling loads for these modes (L_2 , and D_2) are nearly the same as those obtained for L_1 , and D_1 , respectively. The observed local and distortional buckling mode shapes at these minima are shown in Fig. 6(a), and (b), respectively.

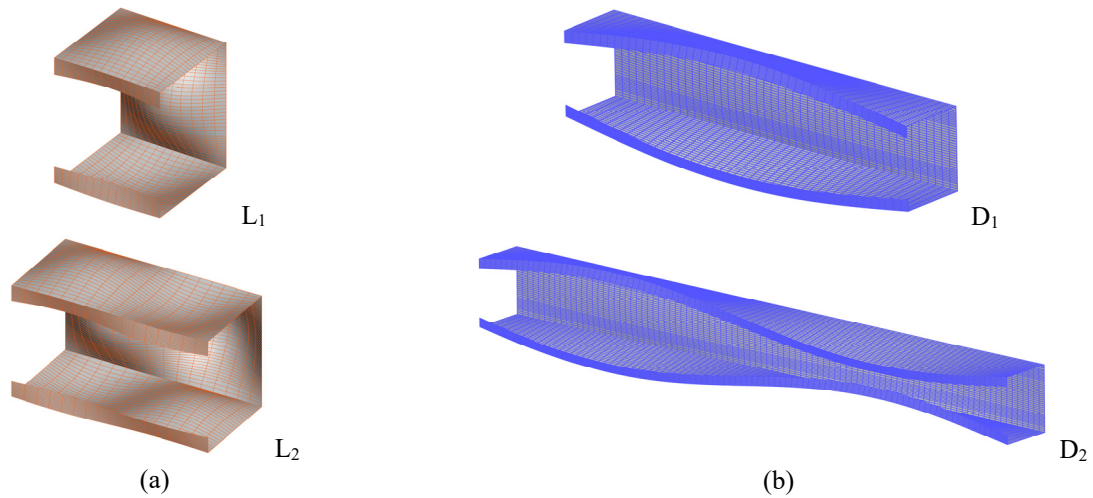


Figure 6: Comparison of (a) local buckling mode shapes; L_1 at $L = 80$ mm, and L_2 at $L = 160$ mm, (b) distortional buckling mode shapes; D_1 at $L = 445$ mm and D_2 at $L = 890$ mm.

5.3 Buckling analysis of built-up I-section

The analysis is focused on single-span built-up columns made from two constituent channel sections connected back-to-back using M4.8 fasteners. The constituent sections are the same as that analyzed in section 5.2. Fig. 7 shows the geometry and FS discretization of the built-up I-section.

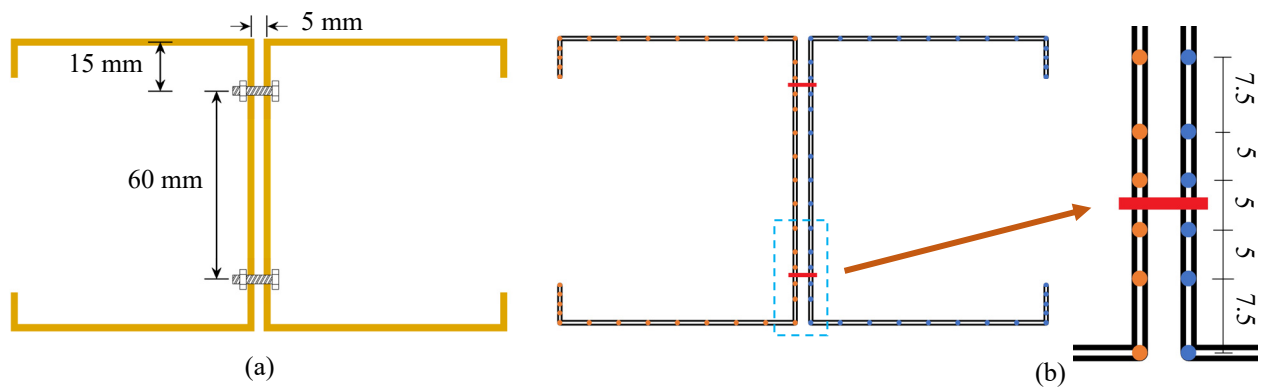


Figure 7: Built-up I-section: (a) geometry and fasteners placement, (b) finite strip discretization.

The fasteners are assumed to be spaced 50 mm apart longitudinally. This spacing is less than typical fastener spacings used in practice, chosen to be shorter than the local buckling half-wavelength so that the fasteners may influence both the local and distortional buckling modes. The distance between the first rows of fasteners and the member ends is set to 5 mm. Thus, the shortest built-up member considered is 60 mm long. The compound finite strip method with 40 longitudinal terms is utilized to analyze the buckling behavior of the considered built-up section. The CSM results are presented in Fig. 8 and compared with the FE solutions obtained using Abaqus. As can be seen, in both the compound strip and finite element analyses, the inclusion of discrete fasteners leads to curves that deviate from the single section curve in the local, distortional and global

buckling regions. It is noted that in the FE buckling analysis, the fastener are modelled using cartesian connection elements with elastic behavior. According to the graphs presented in Fig. 8, a good agreement between the FE and CMS results is achieved.

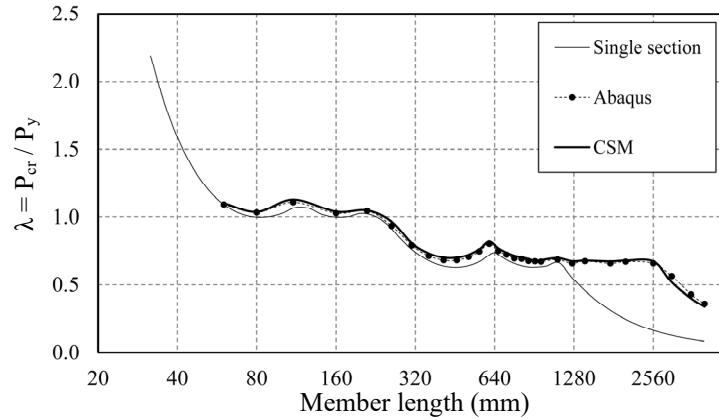


Figure 8: Comparison of buckling load curves of built-up I-section obtained from the compound finite strip and finite element analyses

The buckling mode shapes of the built-up member with lengths of 110 mm, 660 mm, and 3020 mm are shown in Fig. 9, Fig. 10, and Fig. 11, respectively. In the figures, the first buckling mode shapes obtained using CSM are compared with the results of FE analyses. The results in Fig. 9 indicate similar local buckling modes are obtained using FEM and CSM. For $L = 660$ mm, the buckling mode is distortional, and again the FEM and CSM analyses yield similar buckling mode shapes, see Fig. 10. The same applies to the global (torsional) buckling modes obtained for $L = 3020$ mm, as shown in Fig. 11. The agreement between the FEM and CSM results shown in Fig. 8 – Fig. 11, confirm the capability of the proposed CSM analysis to predict the buckling capacity and mode shapes of built-up CFS sections with discrete web fasteners.

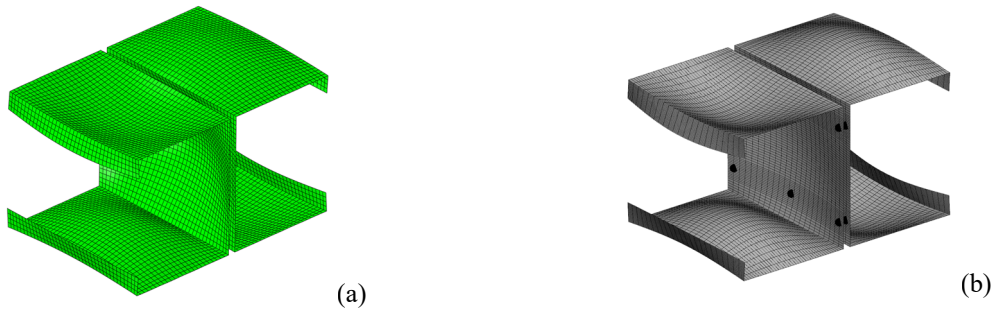


Figure 9: Comparison of the first buckling mode shape of the built-up member at $L = 110$ mm: (a) FEM, (b) CSM.

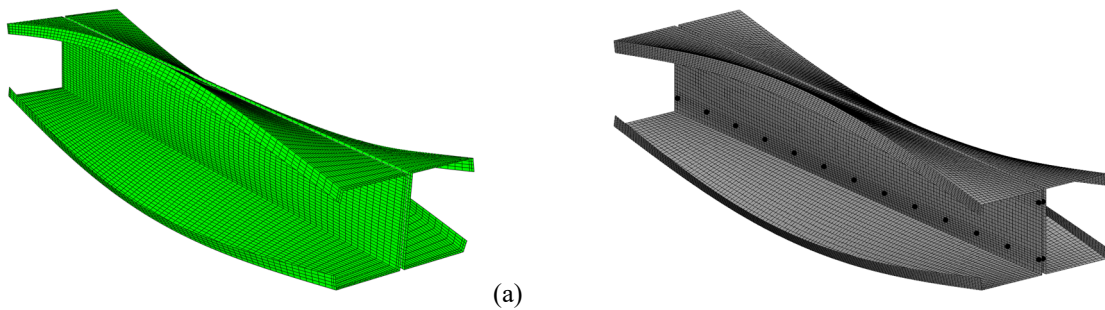


Figure 10: Comparison of the first buckling mode shape of the built-up member at $L = 660$ mm: (a) FEM, (b) CSM.

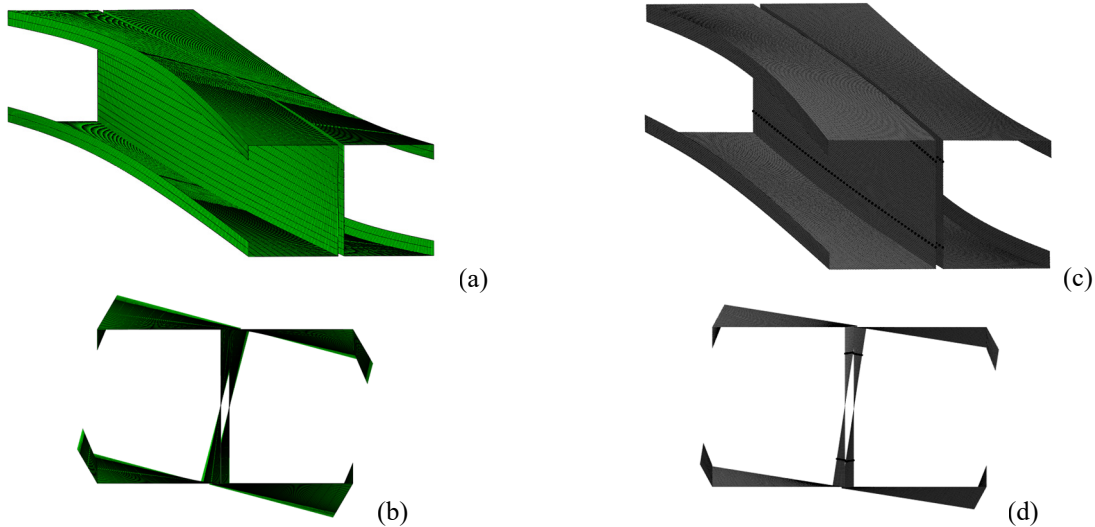


Figure 11: Comparison of the first buckling mode shape of the built-up member at $L = 3020$ mm: (a,b) FEM, (c,d) CSM.

The results presented in Fig. 8 demonstrate that the constituent section (single section) experiences global buckling when the member length exceeds 1100 mm, whereas for the built-up member, global buckling becomes critical when the member length increases above 2500 mm. This confirms the effect of composite action between the constituent sections and highlights the importance of considering the presence of fasteners in the analysis.

5.4 Modal decomposition of buckling modes for single channel section

In this example the critical buckling loads of the lipped C-section columns with the cross-section shown in Fig. 4 are obtained. The material properties are as follows: $E = 210$ GPa, $G = 105$ GPa, $\nu = 0$, and $f_y = 450$ MPa.

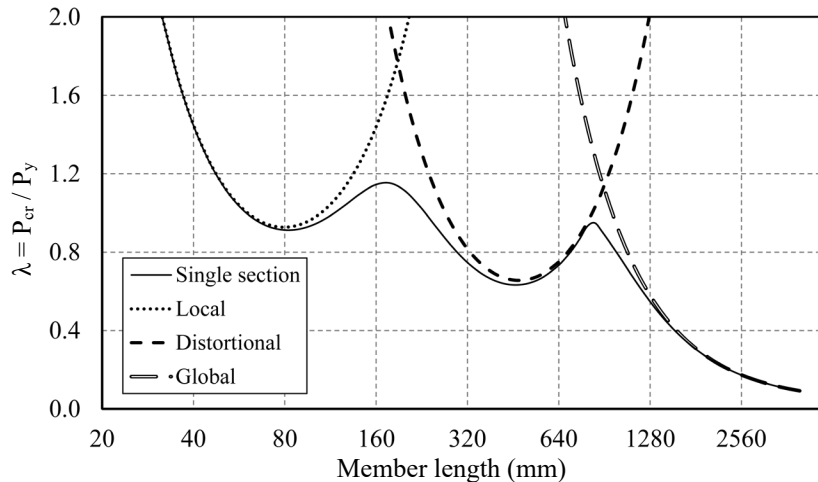


Figure 12: Critical buckling curves for lipped channel columns with pin end conditions using one longitudinal term.

The critical buckling loads for all-modes (solution obtained using Eq. 17) and pure modes calculated for pinned simple support conditions are presented in Fig. 12. Using the signature curve for pin-ended columns, the buckling lengths for the local and distortional minima are obtained as

$L_{Cr,L} = 80 \text{ mm}$ and $L_{Cr,D} = 450 \text{ mm}$, respectively. The results obtained using mFSM for the pure local and distortional deformation modes give identical results, as shown in Fig. 12.

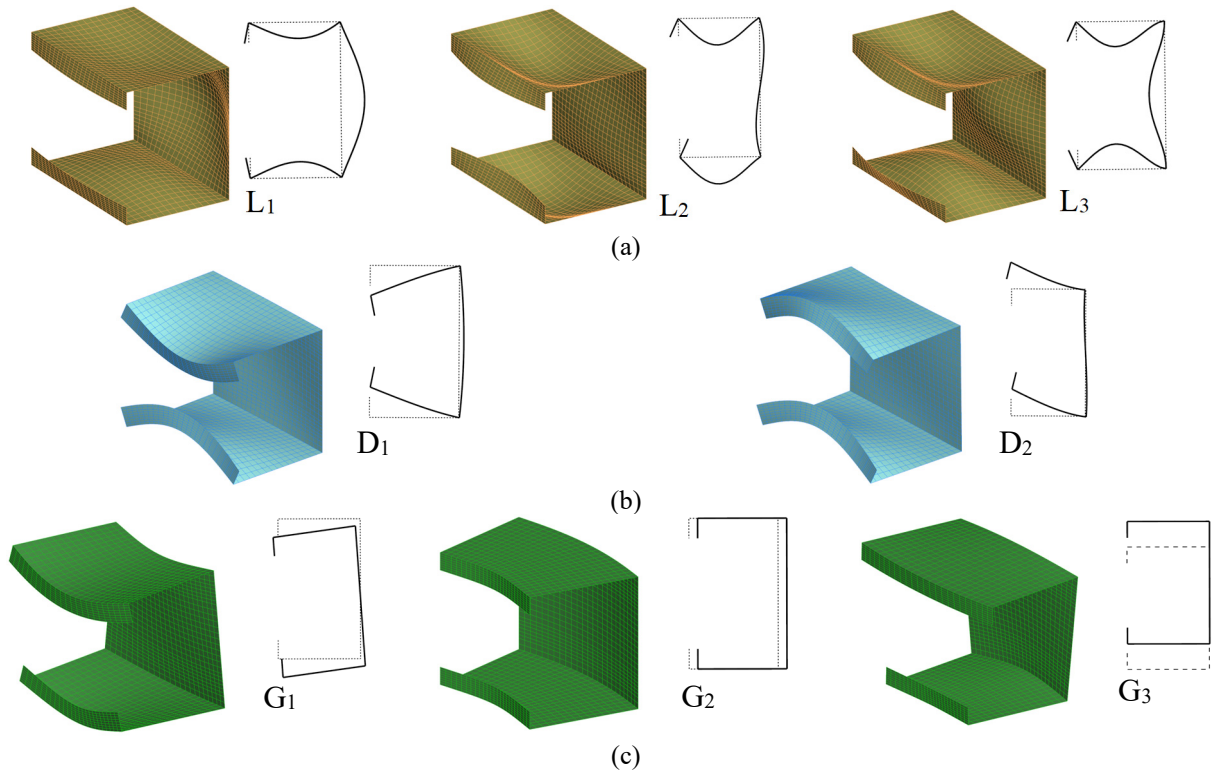


Figure 13: Decomposed mode shapes of single C-section at $L = 110 \text{ mm}$, (a) Local (b) Distortional (c) Global modes

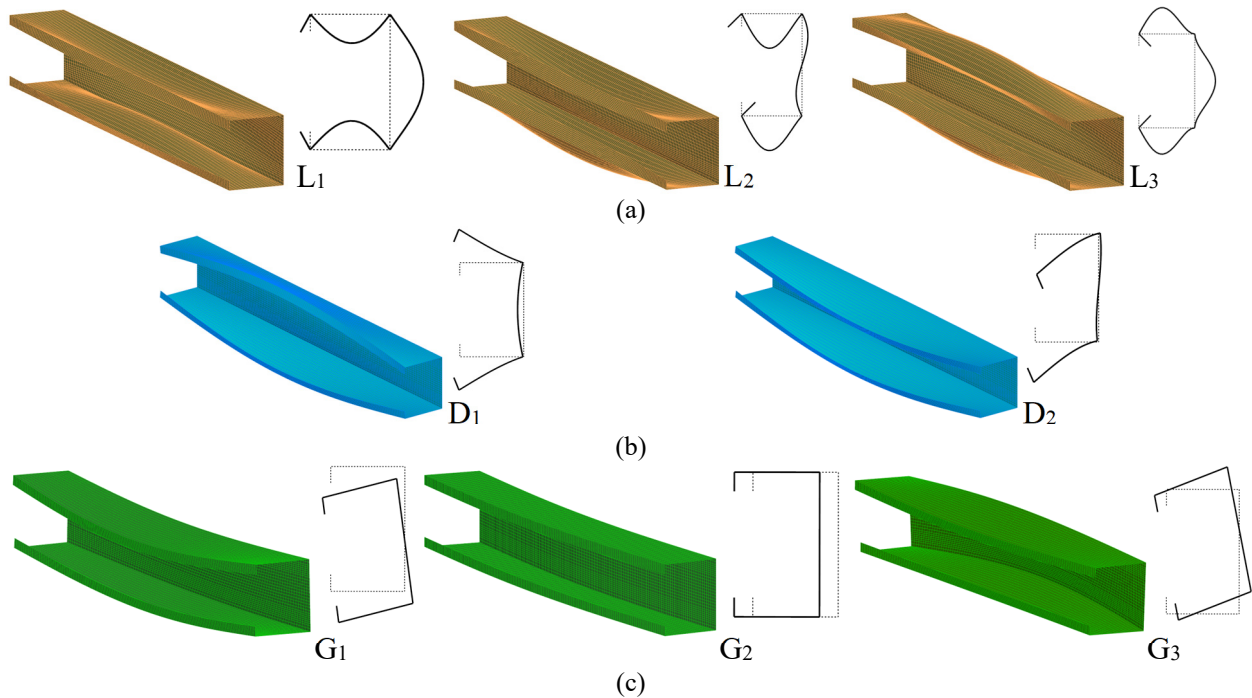


Figure 14: Decomposed mode shapes of single C-section at $L = 660 \text{ mm}$, (a) Local (b) Distortional (c) Global modes

The corresponding pure deformation mode shapes obtained using the mFSM are shown in Fig. 13 and Fig. 14 for the lengths of 110 mm and 660 mm, respectively. As can be seen, only two distortional modes are feasible for the considered section, when only one longitudinal term is used in the analysis. It can be concluded that the mFSM is able to decompose the buckling solution of the section into “pure” modes.

5.5 Modal decomposition of buckling modes for the built-up I-section

This example analyses the built-up I-section column defined in Section 5.2 using the proposed mFSM method. The material constants are as follows: $E = 210$ GPa, $G = 105$ GPa, $\nu = 0$, and $f_y = 450$ MPa. As there are no other numerical methods available to decompose the buckling modes of built-up members with discrete fasteners, the results obtained using mFSM can be only verified by studying the all-mode buckling loads and buckling mode shapes. Comparisons are made with mFSM results obtained for single section to assess the buckling behavior of the built-up member and the obtained pure buckling mode curves.

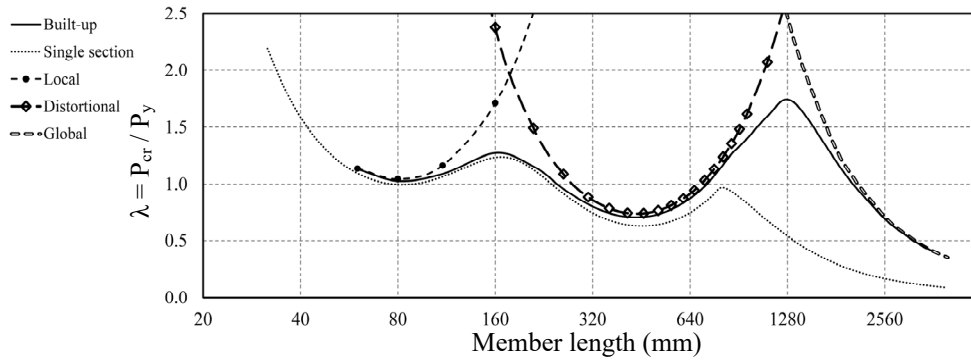


Figure 15: Critical buckling curves for built-up columns with pin-ended support conditions

The normalized critical buckling loads are calculated using the proposed mFSM and presented in Fig. 15. As it can be observed in the local region, the enhancement in the buckling capacity of the built-up member in comparison to the single section is insignificant. The difference is attributed to the small but finite separation of the webs of the two channel sections which produces shear deformations of the fasteners as the web buckles. The closeness of the local buckling loads of the single and built-up sections is in agreement with previous results for built-up sections (Abbasi, Khezri, and Rasmussen 2017; Abbasi et al. 2018; Khezri, Abbasi, and Rasmussen 2017) and analytical studies focused on the influence of fasteners on the buckling load of built-up members (Rasmussen et al. 2020). The pure local buckling mode shapes for the built-up member of length 110 mm are shown in Fig. 16. As it was previously shown in Fig. 9, the critical buckling mode for this length is a local mode. A comparison of the modes shown in Fig. 16 with those shown in Fig. 13(a) for the single section member of the same length reveals that local buckling mode shapes are not discernably influenced by the presence of discrete fasteners. It is also noted that the warping displacement for local modes is negligible and thus the fasteners are not engaged in the longitudinal direction to transfer shear. These observations confirm the mFSM results and the conclusion that the built-up section has similar local buckling capacity as the single section. The pure distortional buckling mode shapes for the same length ($L = 110$ mm) are presented in Fig. 17. It is noteworthy that the number of distortional buckling modes for the built-up member is increased to four modes (here only the first three are shown) from only two modes for the single section. This indicates that the mFSM has correctly picked up other possible distortional modes of the built-up member.

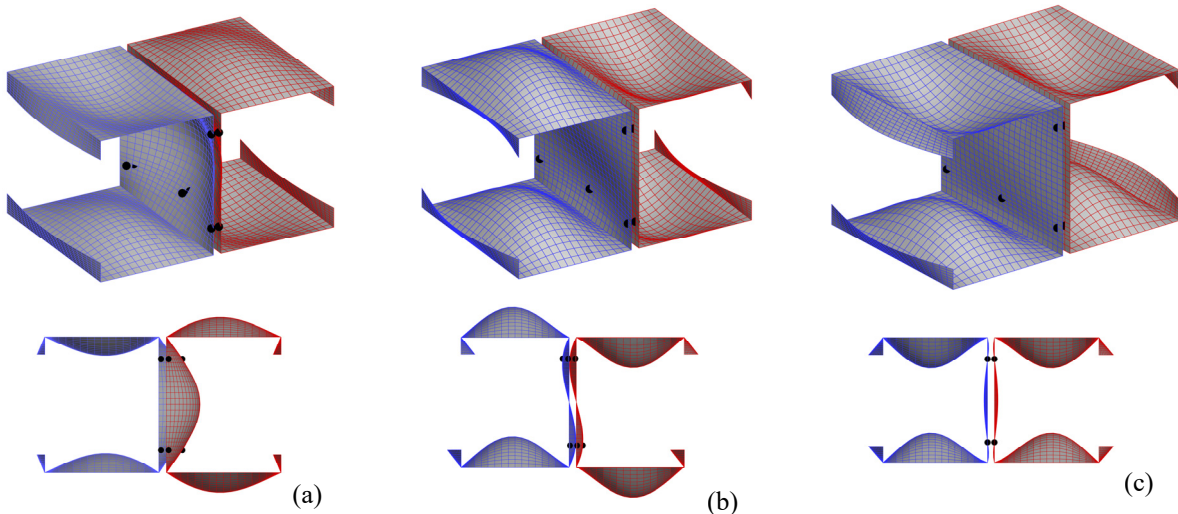


Figure 16: Pure local mode shapes of built-up I-section at length $L= 110$ mm (a) first (b) second, and (c) third modes

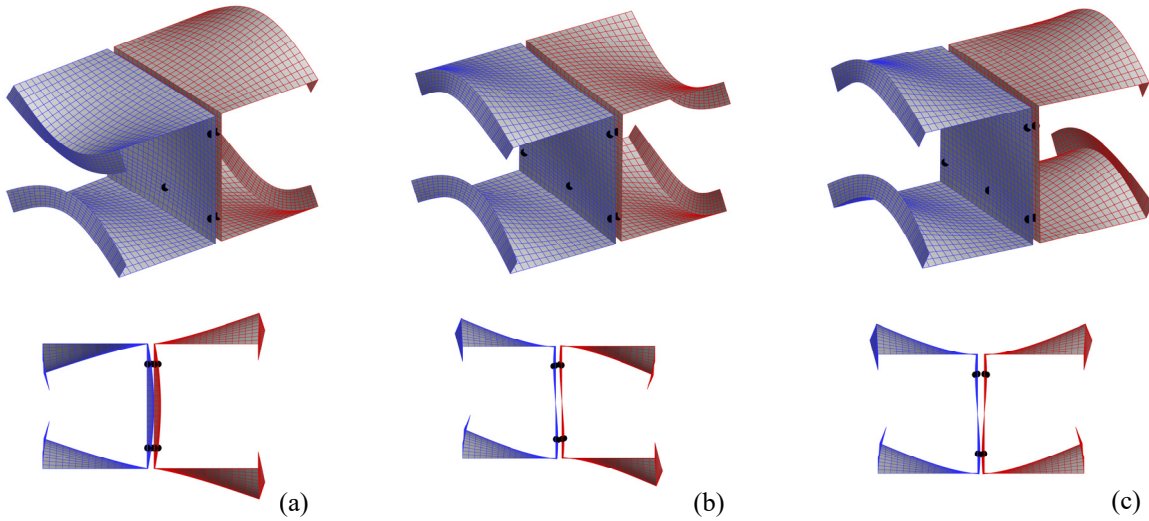


Figure 17: Pure distortional mode shapes of built-up I-section at length $L= 110$ mm (a) first (b) second, and (c) third modes

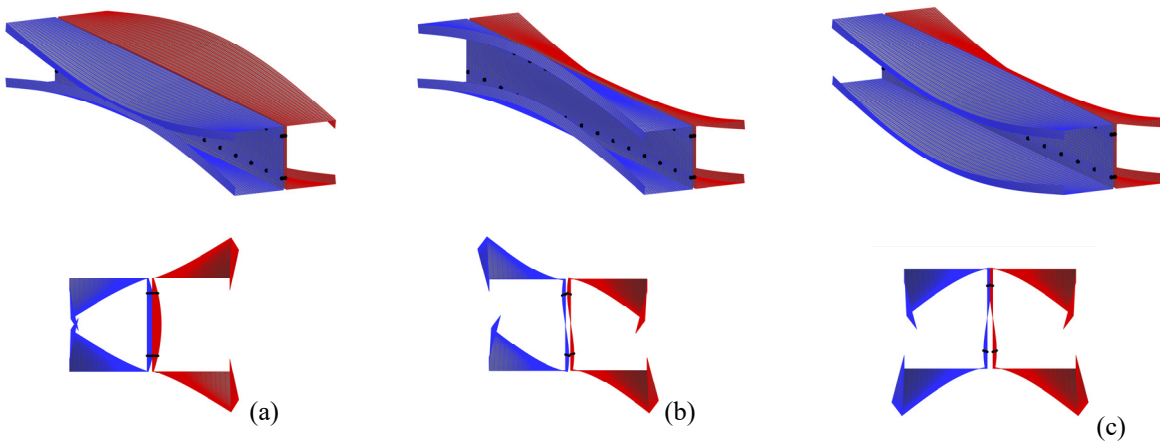


Figure 18: Pure distortional mode shapes of built-up I-section at length $L= 660$ mm (a) first (b) second, and (c) third modes

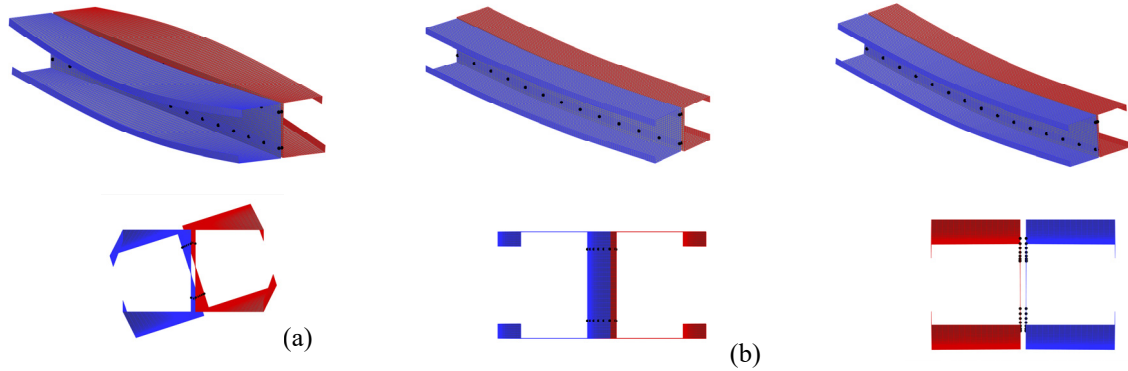


Figure 19: Pure global mode shapes of built-up I-section at length $L= 660$ mm (a) first (b) second, and (c) third modes

The pure distortional and global buckling mode shapes for the built-up member of length 660 mm are shown in Fig. 18 and Fig. 19, respectively. The all-mode buckling analysis of the member of this length presented in Fig. 10 indicates that the critical buckling mode is distortional. As can be seen in Fig. 15, the buckling capacity of the built-up member in the distortional range is enhanced in comparison to the buckling capacity of the single section. In the distortional dominated region of the curve, the enhancement increases as the member length increases. This can be explained by noting that the warping displacements in distortional modes are not negligible and are proportional to the member length. This means that the fasteners are engaged in the longitudinal direction when the member undergoes distortional buckling and therefore, the buckling load is increased. Because of the composite action between the sections, the range over which distortional buckling occurs increases significantly when compared to the single section. The pure uncoupled global buckling modes for this length shown in Fig. 19 are those expected for a doubly symmetric sections and indicate that the mFSM can correctly predict the pure global buckling modes of a built-up member.

6. Conclusions

The paper presents a novel method for calculating “pure” buckling modes for cold-formed steel built-up sections, termed the modal finite strip method (mFSM). It produces the buckling loads and modes of pure local, distortional and global modes, defined to satisfy the specific kinematic constraints of these modes. The method first uses the confined strip method (CSM) to determine the buckling loads and associated buckling modes of a built-up section, accounting for the constraints imposed by discrete fasteners, as previously presented by the authors. It subsequently uses these buckling modes as input to the modal finite strip method (mFSM), also previously developed by the authors, with selective addition of the stiffness terms associated with fasteners..

Examples are provided of CSM and mFSM analyses of a single and a built-up section, constructed from the same lipped channel section, the latter by joining two sections back-to-back to form a complex I-section. The CSM results are shown to agree with results obtained from finite element analyses of the built-up section. The mFSM results of the built-up section are shown to produce the pure modes expected of a doubly symmetric complex I-section.

Acknowledgments

This project was undertaken as a part of Australian Research Council (ARC) Discovery Project DP220103573.

References

Abbasi, M., Khezri, M., Rasmussen, K.J.R., and Schafer, B.W. (2018). “Elastic buckling analysis of cold-formed steel built-up sections with discrete fasteners using the compound strip method”, *Thin-Walled Structures*, 124 58-71.

- Abbasi, M., Khezri, M., Rasmussen, K.J.R. (2017). "On extending the direct strength method to the design of cold-formed steel built-up columns", *ce/papers*, 1 1600-08.
- Ádány, S. (2018). "Constrained shell Finite Element Method for thin-walled members, Part 1: constraints for a single band of finite elements", *Thin-Walled Structures*, 128 43-55.
- Ádány, S., Schafer, B.W. (2008). "A full modal decomposition of thin-walled, single-branched open cross-section members via the constrained finite strip method", *Journal of Constructional Steel Research*, 64 12-29.
- Ádány, S., Schafer, B.W. (2014a). "Generalized constrained finite strip method for thin-walled members with arbitrary cross-section: Primary modes", *Thin-Walled Structures*, 84 150-69.
- Ádány, S., Schafer, B.W. (2014b). "Generalized constrained finite strip method for thin-walled members with arbitrary cross-section: Secondary modes, orthogonality, examples", *Thin-Walled Structures*, 84: 123-33.
- Ádány, S., Silvestre N., Schafer, B.W., Camotim, D. (2009). "GBT and cFSM: two modal approaches to the buckling analysis of unbranched thin-walled members", *Advanced steel construction*, 5 195-223.
- Ádány, S., Visy, D., Nagy R. (2018). "Constrained shell Finite Element Method, Part 2: application to linear buckling analysis of thin-walled member", *Thin-Walled Structures*, 128 56-70.
- Borković, A., Kovačević, S., Milašinović, D.D., Radenković, G., Mijatović, O., Golubović-Bugarski, V. (2017). 'Geometric nonlinear analysis of prismatic shells using the semi-analytical finite strip method', *Thin-Walled Structures*, 117 63-88.
- Borković, A., Mrđa, N., Kovačević, S. (2013). "Dynamical analysis of stiffened plates using the compound strip method", *Engineering Structures*, 50 56-67.
- Bradford, M. A., Azhari, M. (1995). "Buckling of plates with different end conditions using the finite strip method", *Computers & structures*, 56 75-83.
- Chen, C. J., Gutkowski, R.M., Puckett, J.A. (1991). "B-spline compound strip formulation for braced thin-walled structures", *Journal of Structural Engineering*, 117 1303-16.
- Cheung, M. S., Cheung, Y. K. (1971). "Natural vibrations of thin, flat-walled structures with different boundary conditions", *Journal of Sound and Vibration*, 18 325-37.
- Dinis, P. B., Camotim, D., Silvestre, N. (2006). "GBT formulation to analyse the buckling behaviour of thin-walled members with arbitrarily 'branched' open cross-sections", *Thin-Walled Structures*, 44 20-38.
- Gonçalves, R., Ritto-Corrêa, M., Camotim, D. (2010). "A new approach to the calculation of cross-section deformation modes in the framework of generalized beam theory", *Computational Mechanics*, 46 759-81.
- Khezri, M., Abbasi, M., Rasmussen, K.J.R. (2017). "Application of the compound strip method in buckling analysis of cold-formed steel built-up sections", *ce/papers*, 1 1667-76.
- Khezri, M., Rasmussen, K.J.R. (2018). "A generalized strain–energy based approach to buckling mode decomposition of thin-walled members." *In Proceedings of the Eighth International Conference on Thin-Walled Structures*.
- Khezri, M., Rasmussen, K.J.R. (2019a). "An energy-based approach to buckling modal decomposition of thin-walled members with arbitrary cross-sections, Part 2: Modified global torsion modes, examples", *Thin-Walled Structures*, 138 518-31.
- Khezri, M., Rasmussen, K.J.R. (2019b). "An energy-based approach to buckling modal decomposition of thin-walled members with arbitrary cross sections, Part 1: Derivation", *Thin-Walled Structures*, 138 496-517.
- Maleki, S. (1991). "Compound strip method for box girders and folded plates", *Computers & structures*, 40 527-38.
- Plank, R.J., Wittrick, W.H. (1974). "Buckling under combined loading of thin, flat-walled structures by a complex finite strip method", *International Journal for Numerical Methods in Engineering*, 8 323-39.
- Puckett, J.A. (1986). "Application of the compound strip method for the analysis of slab-girder bridges", *Computers & structures*, 22 979-86.
- Puckett, J.A., Gutkowski R. M. (1986). "Compound strip method for analysis of plate systems", *Journal of Structural Engineering*, 112 121-38.
- Puckett, J.A., Wiseman D.L., Chong K.P. (1987). "Compound strip method for the buckling analysis of continuous plates", *Thin-Walled Structures*, 5 383-400.
- Rasmussen, K.J.R., Khezri, M., Schafer, B.W., Zhang, H. (2020). "The mechanics of built-up cold-formed steel members", *Thin-Walled Structures*, 154 106756.
- Rendall, M.A., Hancock G.J., Rasmussen, K.J.R. (2017). "The generalised constrained finite strip method for thin-walled members in shear", *Thin-Walled Structures*, 117 294-302.
- Schafer, B.W., Adany, S. (2006). "Buckling analysis of cold-formed steel members using CUFMS: conventional and constrained finite strip methods." *In 18th international specialty conference on CFS structures*, 39-54.
- Strang, G. (1993). "The fundamental theorem of linear algebra", *The American Mathematical Monthly*, 100 848-55.
- Wiseman, D.L., Puckett, J. A. (1991). "Applications of compound strip method for folded plates with connecting elements", *Journal of Structural Engineering*, 117 268-85.